Evolution of Crystallographic Phases in $(Sr_{1-x}Ca_x)TiO_3$ with Composition (x)

Rajeev Ranjan,* Dhananjai Pandey,*,1 W. Schuddinck,† O. Richard,† P. De Meulenaere,†
J. Van Landuyt,† and G. Van Tendeloo†

*School of Materials Science & Technology, Institute of Technology, Banaras Hindu University, Varanasi 221005, India; and †Electron Microscopy
for Materials Research (EMAT), Universiteit Antwerpen (RUCA), Groenenborgerlaan 171, 2020 Antwerpen, Belgium

Results of X-ray powder diffraction, neutron powder diffraction, electron microdiffraction, and convergent beam electron diffraction (CBED) studies are presented to show that the space group of $(Sr_{1-x}Ca_x)TiO_3$ (SCT) in the composition range $0.35 < x \leq 0.55$ cannot be *Cmcm*. The correct space groups are *Pbcm* for $0.35 < x \leq 0.40$ and *Pbnm* for $0.40 < x \leq 0.55$. The analysis of powder XRD data reveals that the structure of SCT is noncubic for $x \geq 0.06$. It is shown that four different types of orthorhombic phases appear in the SCT system with increasing Ca^{2+} content. © 2001 Academic Press

Key Words: $(Sr_{1-x}Ca_x)TiO_3$; perovskites; electron microdiffraction; CBED; neutron powder diffraction; X-ray powder diffraction; antiferroelectrics; quantum ferroelectrics; tilt transitions.

1. INTRODUCTION

Strontium titanate ($SrTiO_3$) has been the model system for studies related to structural phase transitions and critical phenomena (1–3). Upon lowering of the temperature, the dielectric constant of $SrTiO_3$ gradually increases and becomes nearly 20,000 at 4 K (4). This has been attributed to the softening of a zone-center optical mode. Upon lowering of the temperature below 4 K, the dielectric constant (ε') becomes temperature independent and does not lead to any peak in $\varepsilon'(T)$, indicating the absence of a ferroelectric phase transition (4). This leveling off of the $\varepsilon'(T)$ below 4 K has been attributed to zero-point quantum fluctuations, which preclude the freezing of the soft zone-center optical mode. $SrTiO_3$ has accordingly been termed as a quantum paraelectric or an incipient ferroelectric (4).

A rich variety of phase transitions are known to result when Ca^{2+} is substituted at the Sr^{2+} site in $SrTiO_3$ (5–14). In the $(Sr_{1-x}Ca_x)TiO_3$ (SCT) system, a very small concen-

tration of Ca^{2+} has been shown by Bednorz and Muller (7) to stabilize X–Y-type quantum ferroelectricity above a critical Ca^{2+} concentration of $x_c = 0.0018$. The phase transition behavior changes from quantum to classical type for $x > 0.016$ (7). The peak in the dielectric constant becomes increasingly smeared out with increasing x in the composition range $0.016 < x \leq 0.12$ (7). Ranjan *et al.* (14) have proposed that this smearing is due to a dipole glass/relaxor ferroelectric transition caused by the frustration introduced by competing ferroelectric and antiferroelectric interactions. Ranjan *et al.* (14) have also shown that $(Sr_{1-x}Ca_x)TiO_3$ (SCT) undergoes an antiferroelectric phase transition in the composition range $0.12 < x < 0.43$. For $x \geq 0.43$, SCT exhibits incipient antiferroelectric behavior (15).

In addition to the zone-center soft mode, $SrTiO_3$ has a zone boundary soft mode also. The cubic (space group: $Pm3m$) to tetragonal (space group: $I4/mcm$) phase transition below 105 K in $SrTiO_3$ is driven by the zone boundary R_{25} mode (1). For the SCT system, Ranjan and Pandey (13) have shown that, with increasing Ca^{2+} content, the structural phase transition behavior changes from $SrTiO_3$-like to $CaTiO_3$-like above a critical Ca^{2+} concentration $x \approx 0.12$. $CaTiO_3$, unlike $SrTiO_3$, exhibits an orthorhombic (space group: $Pbnm$) to cubic (space group: $Pm3m$) phase transition mediated by an intermediate tetragonal phase (space group: $I4/mcm$) (16, 17) due to phonon instabilities at the R and M points of the cubic Brillouin zone.

While the phase transition aspects in the SCT system are reasonably well understood, there are several controversies about the room-temperature structure of SCT as a function of Ca^{2+} content. As said earlier, the structure of $SrTiO_3$ at room temperature is cubic (space group: $Pm3m$) whereas $CaTiO_3$ has an orthorhombic structure (space group: $Pbnm$) (18). In the mixed $(Sr_{1-x}Ca_x)TiO_3$ system, it is expected that, above a certain critical Ca^{2+} concentration, the structure will change from cubic to orthorhombic. In an early work, McQuarrie (19) proposed that the structure of SCT changes from cubic to tetragonal for $0.15 < x < 0.55$ and

1 To whom correspondence should be addressed. Fax: 091-542-368147/368428. E-mail: dpandey@banaras.ernet.in.

tetragonal to orthorhombic for $x \geq 0.55$. Mitsui and Westphal (6) investigated the room-temperature structure of SCT in the composition range $0 \leq x \leq 0.20$ and reported that the structure of SCT becomes tetragonal (space group: $I4/mcm$) for $x > 0.10$. Ceh et al. (20) have questioned the existence of the tetragonal phase in the SCT system and have proposed that the cubic–orthorhombic phase boundary is located around $x = 0.40$. Based on the observation of two tilt transitions, Ranjan and Pandey (13) have argued that the structure of SCT should be orthorhombic for $x \geq 0.12$. Further, Ranjan et al. (12) have shown that the structure of SCT for $x = 0.50$ is exactly identical to that of $CaTiO_3$ with the $Pbnm$ space group. McQuarrie (19) and Ball et al. (21) have, on the other hand, proposed that the structure of SCT does not become $CaTiO_3$-like until $x \geq 0.55$. According to Ball et al. (21), SCT has a $Cmcm$ space group in the composition range $0.35 < x \leq 0.55$. As per the phase diagram of SCT given by Ranjan et al. (14, 22), SCT for $0.35 < x \leq 0.40$ is antiferroelectric at room temperature. According to Ranjan et al. (14, 22), the space group of the antiferroelectric phase of SCT is $Pbcm$. This raises doubts about the correctness of the $Cmcm$ space group proposed by Ball et al. (21).

In the present work, we have examined the room-temperature crystal structure of SCT using X-ray powder diffraction, neutron powder diffraction, electron microdiffraction, and convergent beam electron diffraction (CBED) techniques with a view to settle the existing controversies about the structure of SCT as a function of Ca^{2+} content.

2. EXPERIMENTAL

SCT samples were prepared using solid state thermochemical reaction in a stoichiometric mixture of $SrCO_3$, $CaCO_3$, and TiO_2. The powders were mixed in a ball mill using zirconia jars and balls for 6 h. Acetone was used as the mixing media. Calcination of the mixed powder was carried out at $1100°C$ for 6 h. Before pelletization, the calcined powders were ball-milled for 2 h for breaking the agglomerates. Sintering of the pellets was carried out at $1300°C$ for 6 h. The sintered pellets were crushed to fine powders and subsequently annealed at $500°C$ for 12 h for removing the strains induced, if any, during the crushing process before using it for diffraction studies.

X-ray diffraction studies were carried out using a 12-kW Rigaku rotating anode based powder X-ray diffractometer operating in the Bragg–Brentano focusing geometry. Electron microdiffraction and CBED studies were carried out on a Philips 200-kV electron microscope (model CM20). For electron microscopy, the powder was ground in ethanol and the small crystallites were dispersed on a holey carbon grid.

3. X-RAY DIFFRACTION STUDIES

3.1. Superlattice Reflections Due to Octahedral Tilts

Figure 1 depicts powder X-ray diffraction patterns of SCT for $x = 0.00$ (ST), 0.06 (SCT6), 0.09 (SCT9), 0.12 (SCT12), 0.25 (SCT25), 0.30 (SCT30), 0.35 (SCT35), 0.36 (SCT36), 0.40 (SCT40), 0.43 (SCT43), 0.50 (SCT50), and 1.00 (CT) in the 2θ range of $35°–65°$. These patterns have been zoomed to make the superlattice peaks visible. Because of this zooming, some of the main perovskite peaks are truncated in the figure. The superlattice reflections are due to the doubling of the elementary perovskite cell caused by tilting of the TiO_6 octahedra (12). The Miller indices given in Fig. 1 are with respect to a doubled elementary perovskite cell ($2a_p \times 2b_p \times 2c_p$). As shown by Glazer (23, 24), superlattice reflections with all-odd (ooo) Miller indices arise due to "anti-phase" (−) tilting of the neighboring TiO_6 octahedra whereas superlattice reflections with two-odd and one-even (ooe) type Miller indices are due to "in-phase" (+) tilting. The antiparallel displacements of Sr^{2+}/Ca^{2+} ions in the neighboring elementary perovskite cells give rise to superlattice reflections, which are of oee type (23, 24).

It can be seen from Fig. 1 that the superlattice reflections of ooo, ooe, and oee types are present in the XRD patterns of SCT43, SCT50, and $CaTiO_3$. Based on the presence of the three types of superlattice reflections, the tilt system for SCT43 and SCT50 are expected (12) to be identical to that for $CaTiO_3$, that is, $a^-a^-c^+$ (space group: $Pbnm$) (23, 24).

FIG. 1. XRD patterns of different compositions of SCT. The y-axis is zoomed to enable the superlattice reflections to become visible. As a result of this, some of the main perovskite reflections are truncated.

The XRD patterns of SCT compositions with $0.09 < x < 0.36$ contain superlattice reflections of ooo type only. If we assume that ooe type superlattice reflections are truly extinguished, the tilt system for SCT compositions with $0.09 \leq x < 0.36$ would be either $a^0a^0c^-$ (space group: $I4/mcm$), similar to the structure of the low-temperature (<105 K) phase of $SrTiO_3$ (2), or $a^-a^-c^0$ (space group: $Ibmm$) (12). However, the observation (13) of two tilt transitions clearly rules out the possibility of a $a^0a^0c^-$ type single-tilt system for SCT compositions with $x \geq 0.12$. The similarity of the XRD pattern of SCT9 with that of SCT12 suggests that SCT9 may also exhibit two tilt transitions. Thus, the most plausible tilt system for the composition range $0.90 \leq x < 0.36$ is $a^-a^-c^0$ with space group $Ibmm$.

The 311 superlattice reflection, which is the strongest superlattice reflection, is visible in the XRD patterns up to $x = 0.09$, even though its intensity has become extremely low (10^{-4} times the intensity of the strongest perovskite peak 220). Mitsui and Westphal (6) did not observe any of the superlattice reflections, shown in Fig. 1, for the composition range $0 \leq x \leq 0.20$, presumably due to the low resolution of the old diffractometers.

3.2. Superlattice Reflections in $(Sr_{0.64}Ca_{0.36})TiO_3$ (SCT36) and $Sr_{0.60}Ca_{0.40}TiO_3$ (SCT40) Due to Antiferroelectricity

The XRD patterns of SCT36 and SCT40 in Fig. 1 are similar to those for $0.09 \leq x < 0.36$ with one important difference. In addition to the "ooo" type superlattice reflections, the XRD patterns of SCT36 and SCT40 contain extra weak reflections, which are marked with arrows in the figure. Indexing of these extra weak reflections requires doubling along two elementary perovskite cell parameters (a_p, b_p) and quadrupling along the third (c_p), i.e., the multiple elementary perovskite cell is $2a_p \times 2b_p \times 4c_p$. Such a quadrupling of the c parameter of the elementary perovskite unit cell has recently been reported in SCT30 below room temperature by Ranjan et al. (14), who attributed it to the presence of superlattice reflections characteristic of an antiferroelectric phase. As per the phase diagram of Ranjan et al. (14), SCT36 and SCT40 are antiferroelectric, even at room temperature since the corresponding phase transition temperatures lie above the room temperature. The extra weak reflections seen at room temperature in Fig. 1 for SCT36 and SCT40 are therefore due to the antiferroelectric nature of these two compositions at room temperature. The space group of the antiferroelectric phase of SCT has been confirmed to be $Pbcm$ (14, 22).

Ball et al. (21) have assigned the $Cmcm$ space group and $a^0b^+c^-$ tilt system for the composition range $0.35 < x \leq 0.55$. The three orthorhombic unit cell parameters A_o, B_o, C_o for the $Cmcm$ space group are approximately equal to $2a_p, 2b_p$, and $2c_p$, respectively. However, the fact that the extra weak reflections, marked with arrows in

Fig. 1, cannot be indexed with respect to a unit cell that is doubled along a_p, b_p, and c_p, the $a^0b^-c^+$ tilt system and $Cmcm$ space group for SCT36 and SCT40 are ruled out. Hence, the assignment of the $Cmcm$ space group by Ball et al. (21) for the composition range $0.35 < x \leq 0.40$ is incorrect.

4. SPACE GROUP OF $(Sr_{1-x}Ca_x)TiO_3$ IN THE COMPOSITION RANGE $0.40 < x \leq 0.55$

The $Pbcm$ space group for $x > 0.40$ is ruled out since the X-ray powder diffraction patterns for these compositions in Fig. 1 do not contain the extra weak reflections characteristic of the antiferroelectric phase. We now proceed to show that the correct space group of SCT in the composition range $0.40 < x \leq 0.55$ is $Pbnm$, as proposed by Ranjan et al. (12) and not $Cmcm$ proposed by Ball et al. (21). For this, we present the results of neutron diffraction, electron microdiffraction, and CBED studies on SCT50, which is representative of the above-mentioned composition range.

4.1. Neutron Diffraction Study

To make a choice between the $Pbnm$ and $Cmcm$ space groups, we have refined the structure of SCT50 with the $Cmcm$ space group also using the same neutron powder diffraction data that was earlier used by Ranjan et al. (12) for establishing the $Pbnm$ space group.

For Rietveld refinement, the various initial structural parameters were taken from the refined values of Ball et al. (21). The minimum value of the R_{wp} ($=8.07$) was attained after a few cycles of refinement. The refined structural parameters are listed in Table 1. The refined positional coordinates (X, Y, Z) obtained by us are very close to those reported by Ball et al. (21). The isotropic thermal (B) parameters in our case are smaller than those reported by Ball et al. (21) for all the atoms except Sr/Ca(1). The calculated neutron powder diffraction profile for the refined

TABLE 1
Refined Structural Parameters of SCT50 with *Cmcm* Space Group Using Neutron Powder Diffraction Data

Atom	X	Y	Z	B (Å^2)
Sr/Ca(1)	0.0	$-0.001(3)$	0.25	1.6(3)
Sr/Ca(2)	0.0	0.487(2)	0.25	0.1(2)
Ti	0.25	0.25	0.0	0.4(1)
O(1)	0.270(1)	0.0	0.0	0.9(1)
O(2)	0.0	0.225(1)	0.033(2)	0.3(1)
O(3)	0.285(2)	0.261(1)	0.25	0.7(2)

Note. $A_0 = 7.763(2)$ Å, $B_0 = 7.776(1)$ Å, $C_0 = 7.757(2)$ Å, $R_p = 5.92$, $R_{wp} = 8.07$, $R_B = 6.12$, and $R_e = 6.11$.
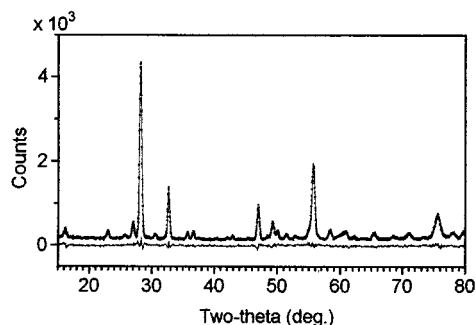
FIG. 2. Observed (...), calculated (——), and difference neutron powder diffraction pattern of SCT50 after final refinement with the *Cmcm* space group.

structure is in good agreement with that experimentally observed, as can be seen from Fig. 2. However, a similar fit is observed even if one does the refinement with the *Pbnm* space group. The goodness-of-fit parameter, R_{wp}, for the *Cmcm* space group ($R_{wp} = 8.07$) is comparable to that obtained by Ranjan *et al.* (12) for the *Pbnm* space group ($R_{wp} = 8.08$). It is, therefore, not possible to make a unique choice between the two space groups, *Cmcm* and *Pbnm*, purely on the basis of Rietveld analysis of powder diffraction data.

The total number of refinable positional coordinates in both *Cmcm* as well as *Pbnm* space groups is seven. Since the number of atoms in the asymmetric unit is six and four for the *Cmcm* and *Pbnm* space groups, respectively, the number of refinable isotropic thermal parameters for the *Cmcm* space group is two more than that for the *Pbnm* space group. Further, the unit cell volume of the *Cmcm* space group is double the unit cell volume of the *Pbnm* space group. As per crystallographic conventions, one chooses the smallest size unit cell representing the lattice symmetry of the crystal. Since no improvement in refinement results with the choice of the *Cmcm* space group, even after using a larger number of refinable parameters and a larger unit cell, it is more appropriate to assign the *Pbnm* space group with a smaller unit cell to SCT50. As shown in the next section, analysis of ZOLZ and FOLZ microdiffraction patterns in conjunction with CBED patterns uniquely fix the *Pbnm* space group for SCT50.

4.2. Electron Diffraction Studies

Electron microdiffraction patterns were recorded with a focused and nearly parallel incoherent beam. These patterns allow one to obtain the crystal system and the Bravais lattice and to reveal the presence of glide planes and screw axes of a crystal. The crystal system is obtained from the electron microdiffraction patterns having the highest "net" symmetry (25). The "net" symmetries take into account the

position (not the intensity) of the reflections on the patterns and hence do not require accurate alignment of a zone axis with respect to the electron beam since a slight misorientation of the diffracted beam does not significantly affect the position of the reflections. The Bravais lattice, the glide planes, and the partial extinction symbols are determined by comparing the experimental patterns with the theoretical ones given by Morniroli and Steeds (25). Taking into account the different possibilities of the Bravais lattices and the glide planes for each crystal system, all the theoretical electron microdiffraction patterns have been computed by Morniroli and Steeds (25). An individual partial extinction symbol is given for each theoretical microdiffraction pattern. By adding one, two, or three individual partial extinction symbols corresponding to different zone-axis patterns (depending on the crystal system), one obtains a small number of possible space groups. Usually, these possible space groups belong to different point groups, which may be distinguished by the study of the positions as well as the intensity distributions of the reflections in the CBED patterns. Recording of the CBED patterns requires a very accurate orientation of the zone axis with respect to the electron beam since the diffracted beam intensity depends greatly on the precise orientation. Using the combination of electron microdiffraction patterns showing the "net" symmetries and CBED patterns showing the "ideal" symmetry, it is possible to identify the unique space group or at least a small subset of consistent space groups.

4.2.1. Electron microdiffraction studies. Figures 3a–3c depict three whole patterns (zero-order Laue zone (ZOLZ) + first-order Laue zone (FOLZ)) obtained for SCT50, exhibiting the 2*mm* highest "net" symmetry, characteristic of the orthorhombic crystal system. To obtain these patterns, the sample is tilted along the zero-order Laue zone mirrors until the first-order Laue zone reflections appear on the pattern. Using the lattice parameters $A_0 = 5.50$ Å, $B_0 = 7.75$ Å, and $C_0 = 5.49$ Å, the zone axes of the three patterns in Figs. 3a–3c were confirmed to be [001], [010], and [100], respectively. This choice of axes (with $C_0 < A_0 < B_0$) is different from those used in the interpretation of neutron diffraction data by Ranjan *et al.* (12) for which $A_0 = 5.50$ Å, $B_0 = 5.49$ Å, and $C_0 = 7.75$ Å (i.e., $B_0 < A_0 < C_0$). For the $B_0 < A_0 < C_0$ choice, the space group symbol is *Pbnm*, whereas for $C_0 < A_0 < B_0$, the space group symbol becomes *Pcmn* (see "International Tables for Crystallography" (26)). The two space group symbols represent the same structure in different settings, i.e., *cab* and *cba* settings for *Pbnm* and *Pcmn*, respectively (26). The theoretically calculated atlas of microdiffraction patterns (25) for the orthorhombic system correspond to the $C_0 < A_0 < B_0$ choice of axes and hence the need to change over from the *Pbnm* space group symbol to the *Pcmn*.
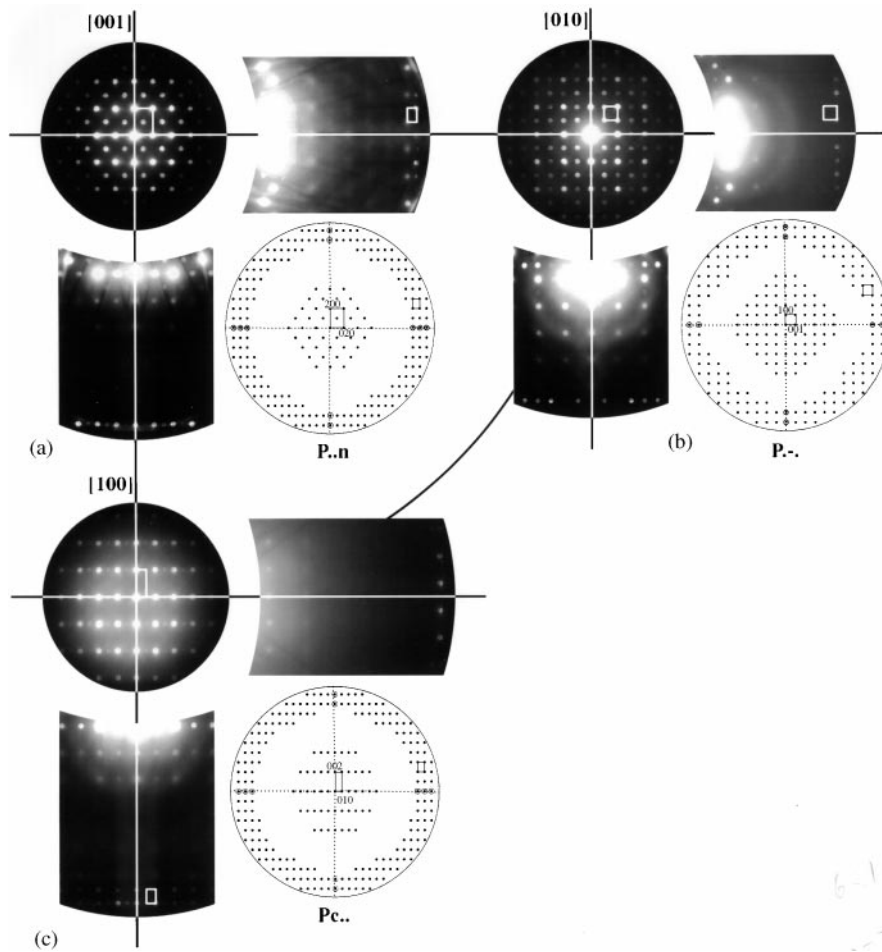
FIG. 3. Electron microdiffraction pattern (ZOLZ + FOLZ) of SCT50 along the (a) [001], (b) [010], and (c) [100] zone axes of the orthorhombic cell.

For an orthorhombic crystal system, the determination of the partial extinction symbol requires analysis of the [001], [010], and [100] zone-axis patterns. On the [001] zone-axis pattern (Fig. 3a), the mesh of reflections of the zero-order Laue zone (ZOLZ) constitutes a centered rectangle. The mesh of reflections of the first-order Laue zone (FOLZ) forms a smaller noncentered rectangle. The periodicity difference between the ZOLZ and FOLZ, plus the change from a centered to a noncentered rectangle is characteristic of the presence of an "*n*" glide plane perpendicular to [001]. Moreover, reflections belonging to the first-order Laue zone are present on the two mirrors. The corresponding theoretical pattern (Fig. 3a) has the individual partial extinction symbol *P..n* where *P* stands for primitive cell and *n* for the *n*-glide plane perpendicular to [001]. The two dots stand for the presence or absence of glide planes to be determined from the [100] and [010] zone-axis microdiffraction patterns. A similar analysis is performed for the [010] and [100] zone-axis patterns. The theoretical patterns corresponding to the experimental ones are presented in Figs. 3b and 3c. The individual partial extinction symbols are *P.-.* and *Pc..*

for the [010] and [100] zone-axis patterns, respectively. The addition of these individual partial extinction symbols leads to the *Pc-n* partial extinction symbol. This symbol, according to the "International Tables of Crystallography" (26), is in agreement with the $Pc2_1n$ (*m2m* point group) and *Pcmn* (*mmm* point group) space groups. Thus, electron microdiffraction studies suggest that the space group of SCT50 can be either *Pcmn* or $Pc2_1$n.

4.2.2. *Convergent beam electron diffraction (CBED) study.* The point group of a crystal system can be determined by observing the "ideal" symmetries of CBED zone-axis patterns. As said earlier, these symmetries take into account the position and the intensity of the reflections. For SCT50, the zero-order Laue zone ideal symmetry of the [001] zone-axis pattern (Fig. 4a) is (2*mm*). The zero-order Laue zone ideal symmetry of the [012] zone-axis pattern is also (2*mm*) (Fig. 4b) and that of the [212] zone-axis pattern (Fig. 4c) is (2). According to Table 2, which gives the ZOLZ and the whole pattern ideal symmetry for the different
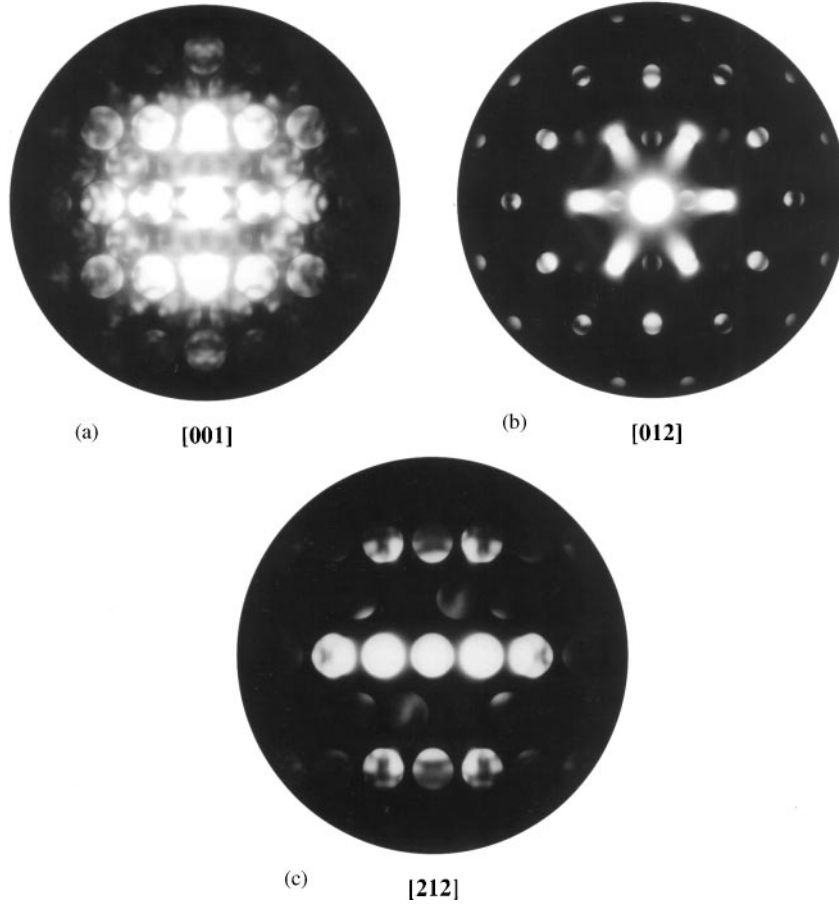
(a) **[001]**

(b) **[012]**

(c) **[212]**

FIG. 4. Convergent beam electron diffraction pattern of SCT50 along (a) [001], (b) [012], and (c) [212] zone axes.

zone-axis patterns and for the different point groups belonging to the orthorhombic crystal system (25), these observed symmetries are in agreement with the *mmm* point group only. This rules out the $Pc2_1n$ space group for the SCT50 for which the point group symmetry is *m2m*. The *Pcmn* space group, on the other hand, has the point group symmetry *mmm*. Thus, the space group of SCT50 is uniquely established as *Pcmn* (or equivalently *Pbnm* in a different setting of the axes).

*4.2.3. Pcmn versus Cmcm in SCT*50. The [010] direction of the *Pcmn* space group is along the $\langle 100 \rangle_p$ of the elementary perovskite cell while [100] and [001] are 45° rotated with respect to the corresponding elementary perovskite cell directions. For the *Cmcm* space group, all three $\langle 100 \rangle$ directions are along the elementary perovskite cell axes $\langle 100 \rangle_p$. Thus, the [010] direction of the *Pcmn* can be parallel to any one of the three $\langle 100 \rangle$ directions of the *Cmcm* space group. Considering only the right-handed coordinate system, the following orientation relationships become possible between the unit cells for the *Pcmn* and *Cmcm* space groups:

(i) $[010]_P \| [010]_C$, $[100]_P \| [1\,0\,\bar{1}]_C$, $[001]_P \| [1\,0\,1]_C$;

(ii) $[010]_P \| [100]_C$, $[100]_P \| [0\,\bar{1}\,1]_C$, $[001]_P \| [0\,1\,1]_C$;

(iii) $[010]_P \| [001]_C$, $[100]_P \| [\bar{1}\,1\,0]_C$, $[001]_P \| [1\,1\,0]_C$.

TABLE 2
"Ideal" Symmetries of the Different Zone-Axis Patterns for the Different Point Groups Belonging to the Orthorhombic Crystal System

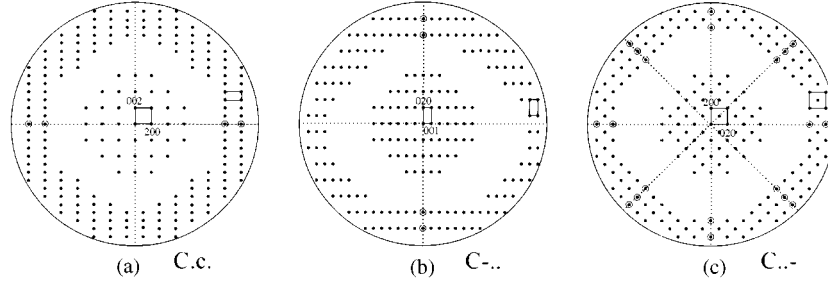| Ortho rhombic	[001]	[010]	[100]	[uv0]	[u0w]	[0vw]	[uvw]
mmm	(2mm)	(2mm)	(2mm)	(2mm)	(2mm)	(2mm)	(2)
	2mm	2mm	2mm	m	m	m	1
2mm	(m)	(m)	(2mm)	(m)	(m)	(m)	(1)
	m	m	2mm	m	m	1	1
m2m	(m)	(2mm)	(m)	(m)	(m)	(m)	(1)
	m	2mm	m	m	1	m	1
mm2	(2mm)	(m)	(m)	(m)	(m)	(m)	(1)
	2mm	m	m	1	m	m	1
222	(2mm)	(2mm)	(2mm)	(m)	(m)	(m)	(1)
	2	2	2	1	1	1	1

FIG. 5. ZOLZ and FOLZ microdiffraction pattern for (a) *C.c.*, (b) *C-..*, and (c) *C..-* partial extinction symbols.

The subscripts P and C refer to the *Pcmn* and *Cmcm* space groups, respectively.

For the possibility (i), there is a *c*-glide perpendicular to [010] for the *Cmcm* space group. The theoretically calculated microdiffraction pattern for *C.c.* partial extinction symbol is shown in Fig. 5a. The two rectangles in ZOLZ and FOLZ, drawn by joining adjacent diffraction spots, in Fig. 5a do not match with the corresponding rectangles shown in Fig. 3b. Moreover, the FOLZ is shifted in such a way that along one of the ZOLZ mirrors (along [001]*) no FOLZ reflections are present. This is not the case for the *P.-.* partial extinction symbol (Fig. 3b) where there are FOLZ reflections on both ZOLZ mirrors. This rules out the *C.c.* partial extinction symbol for Fig. 3b.

Next, we consider the second orientation relationship (ii) for which the partial extinction symbol should be *C-...* The theoretical microdiffraction pattern for this is given in Fig. 5b. Again, the rectangles do not match with the corresponding rectangles in Fig. 3b and also the FOLZ is shifted in such a way that along one of the ZOLZ mirrors (along [001]*) no FOLZ reflection is present. This rules out *C-..* partial extinction symbol for Fig. 3b. It should be noted that the 100 and 001 reflections of the *Pcmn* (see Fig. 3b), becomes $0\bar{1}1$ and 011 reflections for the *Cmcm* space group after unit cell transformation. For the *Pcmn* space group, the 100 and 001 reflections are kinematically forbidden but appear in Fig. 3b by multiple diffraction. On the other hand, the $0\bar{1}1$ and 011 reflections for *Cmcm*, obtained after unit cell transformation, belong to extinct reflections due to *C* centering. Such extinct reflections due to lattice centering cannot appear by multiple diffraction (25).

For the third possible orientation relationship (iii), the partial extinction symbol is *C..-*. The theoretically calculated microdiffraction pattern for *C..-* is shown in Fig. 5c, which is, when turned over 45°, similar to that observed for the *P.-.* partial extinction symbol in Fig. 3b. After unit cell transformation the 200 and 020 reflections of the *Cmcm* become, respectively, 101 and $10\bar{1}$ in the *Pcmn* space group and the 110 and $1\bar{1}0$ reflections become 100 and 001, respectively. Also, the FOLZ reflections are not shifted. Along both ZOLZ mirrors, the FOLZ reflections are present. This

means that similar diffraction patterns will be obtained for the [010] *Pcmn* structure and the [001] *Cmcm* structure. So the *C..-* partial extinction symbol of Fig. 5c cannot be ruled out. The only difference is that the patterns in 3a and 3c cannot be explained with the *Cmcm* description.

The above analysis leads us to the conclusion that the space group of SCT50 cannot be *Cmcm*. Thus, the proposition of Ball *et al.* (21) that the space group of SCT50 is *Cmcm* is incorrect. The correct space group of SCT50 is *Pcmn* (or *Pbnm* in the *cab* setting of the orthorhombic axes), as already established in the previous section.

5. COMPOSITION DEPENDENCE OF ORTHORHOMBIC UNIT CELL PARAMETERS

The room-temperature orthorhombic cell parameters (A_0, B_0, C_0) of SCT in the composition range $0.09 \leq x \leq 0.50$ are related to the equivalent elementary perovskite cell parameters (a_p, b_p, c_p) as under

$$A_0 \approx \sqrt{2}a_p, \quad B_0 \approx \sqrt{2}b_p, \quad \text{and} \quad C_0 \approx 2c_p$$

(For $0.09 \leq x \leq 0.50$ except for $0.36 \leq x \leq 0.40$) [1]

$$A_0 \approx \sqrt{2}a_p, \quad B_0 \approx \sqrt{2}b_p, \quad \text{and} \quad C_0 \approx 4c_p$$

(For $0.36 \leq x \leq 0.40$). [2]

The development of the orthorhombic structures in the SCT system may be visualized to occur in two ways: (i) the elementary cubic perovskite cell may become distorted in a pseudotetragonal sense ($a_p \approx b_p \neq c_p$, $\alpha = \beta = \gamma = 90°$) or (ii) the elementary cubic perovskite cell is monoclinically distorted as in CaTiO$_3$ ($a_p = b_p \neq c_p$, $\alpha = \beta = 90°$, $\gamma \neq 90°$). For the pseudotetragonal distortion, the profile of the *hhh* type reflections in the diffraction patterns will remain a singlet while the *h00* type reflections will be split into two, where the Miller indices *hhh* and *h00* are with respect to the elementary cubic perovskite cell. For monoclinic distortion of the elementary cubic perovskite cell, the *hhh* type reflections will also be split.
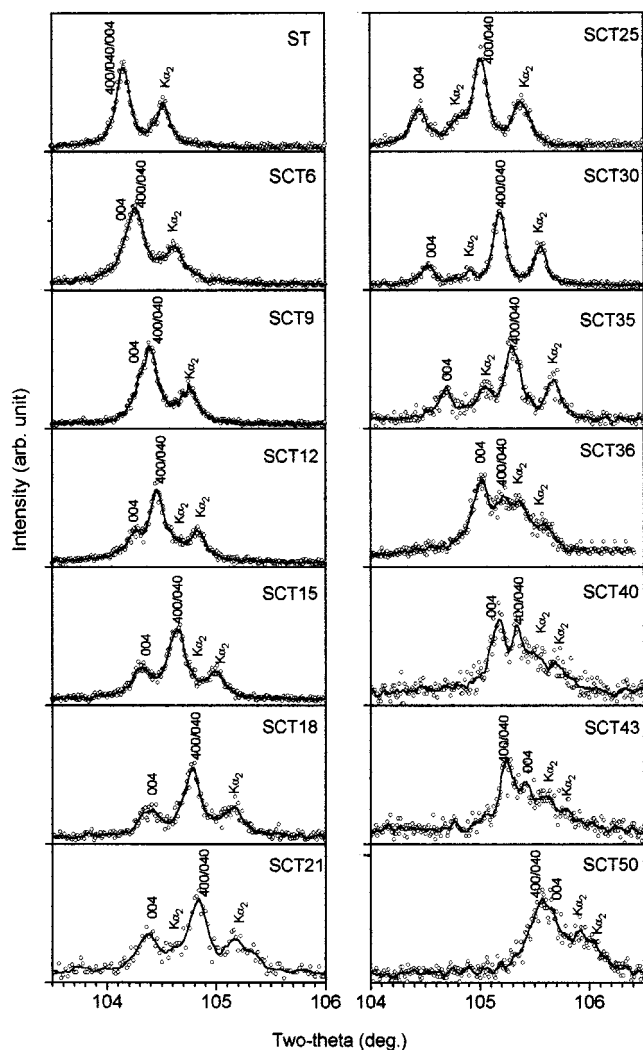
FIG. 6. XRD profile of {400} elementary perovskite reflection for different SCT compositions. The indices are with respect to the elementary perovskite cell.

FIG. 7. Variation of the magnitude of 2θ difference between 004 and 400/040 pair of elementary perovskite reflections with x.

$x = 0.055$. This is, therefore, the critical composition above which the structure of SCT should become noncubic at room temperature, confirming our conclusion about the noncubic structure of SCT6 on the basis of the peak broadening shown in Fig. 6. For $x > 0.35$, the difference $\Delta(2\theta)$ decreases abruptly due to the sudden decrease of the c_p parameter in the antiferroelectric phase of SCT (14, 22). Granicher and Jakits (5) in their low-resolution XRD work called this phase "nearly cubic", which we now know to be orthorhombic (14, 22).

Table 3 gives the refined values of the orthorhombic cell parameters (A_0, B_0, C_0) for $x \geq 0.09$. The equivalent elementary perovskite cell parameters (a_p, b_p, c_p) can be obtained from $A_0, B_0,$ and C_0 values using Eqs. [1] and [2] for the appropriate composition range. The $a_p, b_p,$ and c_p values are plotted as a function of composition in Fig. 8. The equivalent elementary perovskite cell parameters show a pseudotetragonal relationship $(a_p \approx b_p)$.

Figure 6 depicts the XRD profiles for the 400 type elementary perovskite reflections for the composition range $0.0 \leq x \leq 0.50$. It is evident from this figure that these reflections appear as a doublet for all the compositions in the range $0.09 \leq x \leq 0.50$, as expected for the pseudotetragonal elementary perovskite cell. Even for SCT6, the structure seems to be noncubic. This is because the 400 reflection of SCT6 is much broader than that of $SrTiO_3$ (ST). Evidently, the 004 and the 400/040 reflections are not superimposed in SCT6 also.

The variation of the difference between the 2θ angles for the 004 and 400/040 reflections $(\Delta(2\theta) = 2\theta_{400} - 2\theta_{004})$ with Ca^{2+} content (x) is shown in Fig. 7. This difference $(\Delta(2\theta))$ gradually increases with increasing Ca^{2+} content from $x = 0.09$ to $x = 0.35$. Extrapolation of $\Delta(2\theta)$ versus x curve to $\Delta(2\theta) = 0$ intersects the composition (x) axis at
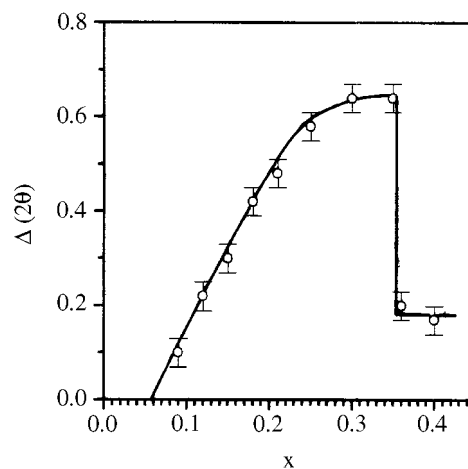
TABLE 3
Refined Orthorhombic Unit Cell Parameters and Unit Cell Volume of $Sr_{1-x}Ca_xTiO_3$

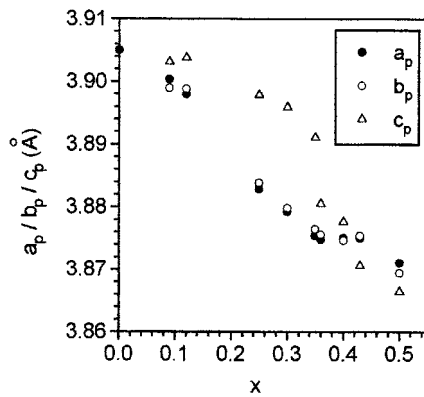| x	A_0 (Å)	B_0 (Å)	C_0 (Å)	V_0 (Å^3)
1.00	5.3783(1)	5.4395(1)	7.6381(2)	223.45
0.50	5.4737(1)	5.4714(1)	7.7329(2)	231.59
0.43	5.4793(2)	5.4798(2)	7.7412(2)	232.43
0.40	5.4793(2)	5.4788(3)	15.5106(5)	465.62
0.36	5.4790(3)	5.4801(2)	15.5222(5)	466.06
0.35	5.4798(1)	5.4813(1)	7.7820(2)	233.74
0.30	5.4853(1)	5.4861(1)	7.7917(2)	234.47
0.25	5.4903(1)	5.4917(1)	7.7956(2)	235.04
0.12	5.5117(2)	5.5129(3)	7.8075(2)	237.23
0.09	5.5151(3)	5.5131(4)	7.8062(4)	237.34

FIG. 8. Variation of equivalent elementary perovskite cell parameters with Ca^{2+} concentration (x).

In the composition range $0.09 \leq x \leq 0.40$, the 004 peak occurs on the lower angle side of 400/040 position, indicating $c_p > a_p$. For $x > 0.40$, this situation is reversed since the 004 peak now occurs on the higher angle side of the 400/040 position. Thus, for $x \leq 0.40$, $c_p > a_p$ whereas for $x > 0.40$, $c_p < a_p$. As per the work of Ball *et al.* (21), the latter trend may continue up to $x \approx 0.55$. For $x > 0.55$, the elementary perovskite cell is monoclinically distorted in the sense discussed earlier.

On the basis of the equivalent elementary perovskite cell parameters (a_p, b_p, c_p) and their relationship with the orthorhombic unit cell parameters (A_0, B_0, C_0), four different types of orthorhombic phases need to be distinguished in the SCT system: (i) Orthorhombic (OI) for $0.09 \leq x < 0.36$: In this composition range, the equivalent elementary perovskite cell is pseudotetragonal with $c_p > a_p(\approx b_p)$, $A_0 \approx B_0 \approx \sqrt{2}a_p$, $C_0 \approx 2c_p$ and the space group is *Ibmm*. (ii) Orthorhombic (OII) for $0.36 \leq x \leq 0.40$: In this composition range, the equivalent elementary perovskite cell is pseudotetragonal with $c_p > a_p(\approx b_p)$, $A_0 \approx B_0 \approx \sqrt{2}a_p$, $C_0 \approx 4c_p$ and its space group is *Pbcm*. (iii) Orthorhombic (OIII) for $0.40 < x \leq 0.55$: In this composition range, the equivalent elementary perovskite cell is pseudotetragonal with $c_p < a_p(\approx b_p)$, $A_0 \approx B_0 \approx \sqrt{2}a_p$, $C_0 \approx 2c_p$ and the space group is *Pbnm*($\equiv$ *Pcmn*). (iv) Orthorhombic (OIV) for $0.55 < x \leq 1.00$: In this composition range, according to Ball *et al.* (21), the equivalent elementary perovskite cell is monoclinically distorted with $a_p = b_p \neq c_p$ with γ_p slightly greater than 90° while the space group remains *Pbnm*.

6. CONCLUSION

Five different phases appear at room temperature as a function of Ca^{2+} content: (i) cubic for $x < 0.06$, (ii) ortho-rhombic phase OI for $0.09 \leq x < 0.36$, (iii) orthorhombic phase OII for $0.36 \leq x \leq 0.40$, (iv) orthorhombic phase OIII for $0.40 < x \leq 0.55$, and (v) orthorhombic phase OIV for $x > 0.55$. The structure of SCT in the composition range $0.06 \leq x < 0.09$ may be either tetragonal or orthorhombic but it is definitely noncubic.

Rietveld analysis of neutron powder diffraction data is of little help in making a choice between the two plausible space groups (*Pbnm* and *Cmcm*) in the composition range $0.40 < x \leq 0.55$. The electron microdiffraction and convergent beam electron diffraction studies have revealed that the correct space group of SCT in this composition range is *Pbnm* (tilt system $a^-a^-c^+$) and not *Cmcm* (tilt system $a^0b^+c^-$). For the composition range $0.36 \leq x \leq 0.40$, the correct space group is *Pbcm*.

REFERENCES

1. G. Shirane and Y. Yamada, *Phys. Rev.* **177,** 858 (1969).
2. A. D. Bruce and R. A. Cowley *Adv. Phys.* **29,** 219 (1980).
3. K. A. Muller, W. Berlinger, and E. Tosatti, *Z. Phys. B: Condens. Matter* **84,** 277 (1991).
4. K. A. Muller and H. Burkard, *Phys. Rev. B* **19,** 3593 (1979).
5. H. Granicher and O. Jakits, *Nuovo Cimento* **9** (Suppl), 480 (1954).
6. T. Mitsui and W. B. Westphal, *Phys. Rev.* **124,** 1354 (1961).
7. J. G. Bednorz and K. A. Muller, *Phys. Rev. Lett.* **52,** 2289 (1984).
8. J. Dec, W. Kleemann, U. Bianchi, and J. G. Bednorz, *Europhys. Lett.* **29**(1), 31 (1995).
9. W. Kleeman, U. Bianchi, A. Burgel, M. Prasse, and J. Dec, *Phase Trans.* **55,** 57 (1995).
10. W. Kleeman, A. Albertini, Chamberlin, and J. G. Bednorz, *Europhys. Lett.* **37**(2), 145 (1997).
11. W. Kleeman, J. Dec, and B. West Wanski, *Phys. Rev. B* **58,** 8985 (1998).
12. R. Ranjan, D. Pandey, V. Siruguri, P. S. R. Krishna, and S. K. Paranjpe, *J. Phys.: Condens. Matter* **11,** 2233 (1999).
13. R. Ranjan and D. Pandey, *J. Phys.: Condens. Matter* **11,** 2247 (1999).
14. R. Ranjan, D. Pandey, and N. P. Lalla, *Phys. Rev. Lett.* **84,** 3726 (2000).
15. S. K. Mishra, R. Ranjan, and D. Pandey, to be published.
16. R. A. Redfern, *J. Phys.: Condens. Matter* **8,** 8267 (1996).
17. B. J. Kennedy, C. J. Howard, and B. C. Chakoumakos, *J. Phys.: Condens. Matter* **11,** 1479 (1999).
18. H. F. Kay and P. C. Bailey, *Acta Crystallogr. B* **10,** 219 (1957).
19. M. McQuarrie, *J. Am. Ceram. Soc.* **38,** 444 (1955).
20. M. Ceh, D. Kolar, and L. Golic, *J. Solid State Chem.* **68,** 68 (1987).
21. C. J. Ball, B. D. Begg, D. J Cookson, G. J. Thorogood, and E. R. Vance, *J. Solid State Chem.* **139,** 238 (1998).
22. R. Ranjan and D. Pandey, *J. Phys.: Condens Matter* **13,** 4251 (2001).
23. A. M. Glazer, *Acta. Crystallogr. B* **28,** 3384 (1972).
24. A. M. Glazer, *Acta. Crystallogr. A* **31,** 756 (1975).
25. J. P. Morniroli and J. W. Steeds, *Ultramicroscopy* **45,** 219 (1992).
26. "International Tables for Crystallography." Kluwer, Dordrecht, 1992.